Reconstitution of autophagosomal membrane tethering reveals that the ability of Atg11 to bind membranes is important for mitophagy.

Devika Andhare[1], Sarah Katzenell[1], Sarah I Najera[2], Katherine M Bauer[2] and Michael J Ragusa[*1,2]

[1]Department of Chemistry, Dartmouth College, Hanover, NH 03755, USA

[2]Department of Biochemistry and Cell Biology, Geisel School of Medicine, Dartmouth College, Hanover, New Hampshire 03755, United States.

[*] Correspondence: michael.j.ragusa@dartmouth.edu

ABSTRACT

Autophagy is essential for the degradation of mitochondria from yeast to humans. Mitochondrial autophagy in yeast is initiated when the selective autophagy scaffolding protein Atg11 is recruited to mitochondria through its interaction with the selective autophagy receptor Atg32. This also results in the recruitment of small 30 nm vesicles that fuse to generate the initial autophagosomal membrane. We demonstrate that Atg11 can bind to autophagosomal-like membranes in vitro in a curvature dependent manner via a predicted amphipathic helix. Deletion of the amphipathic helix from Atg11 results in a delay in mitophagy in yeast. Furthermore, using a novel biochemical

approach we demonstrate that the interaction between Atg11 and Atg32 results in the tethering of autophagosomal-like vesicles to giant unilamellar vesicles containing a lipid composition designed to mimic the outer mitochondrial membrane. Taken together our results demonstrate an important role for autophagosomal membrane binding by Atg11 in the initiation of mitochondrial autophagy.

ABBREVIATIONS

Atg11: autophagy related 11; Atg32: autophagy related 32; DLS: dynamic light scattering; GLT: GUV liposome tethering assay; GUV: giant unilamellar vesicle; EEA1: early endosome antigen1; PE: phosphatidyl ethanolamine; PI3P: phosphatidyl inositol 3-phosphate; PM: plasma membrane; SAR: selective autophagy receptor; YPL: yeast polar lipids

30 # INTRODUCTION

31 Macroautophagy, hereafter autophagy, is the cellular process in which double-membrane vesicles,
32 termed autophagosomes, are generated around cytosolic material leading to their capture within
33 these vesicles[1]. Completed autophagosomes fuse with the vacuole, in yeast, or lysosomes, in higher
34 eukaryotes, leading to the degradation of the captured contents. Autophagy can capture and
35 degrade a wide range of cytosolic material including protein aggregates, intracellular pathogens
36 and membrane-bound organelles. As such, autophagy is essential to maintain cellular homeostasis
37 and also serves as an integral component of innate immunity[2,3].

38

39 Cargo selection during autophagy can occur via a non-selective or selective mechanism[4]. In
40 selective autophagy, cargos are marked as targets for autophagy by selective autophagy receptors
41 (SARs)[5]. SARs are either soluble cytosolic proteins that commonly recognize ubiquitin moieties
42 on the cargo to be degraded or, in the case of membrane-bound organelles, they can also be integral
43 membrane proteins in the membrane of the organelle to be degraded. To initiate selective
44 autophagy, SARs recruit the selective autophagy scaffolding protein Atg11, in yeast, or FIP200,
45 in higher eukaryotes, to the cargo to be degraded[6]. In yeast, Atg11 also binds to Atg9, an integral
46 membrane protein embedded in 30 nm vesicles that serve as the initial membrane source for
47 autophagy[7-9]. Once recruited to the cargo, Atg9 vesicles fuse to generate an initial membrane sheet,
48 termed the phagophore[10]. The phagophore expands around the cargo through lipid transport from
49 Atg2 in addition to other mechanisms[11-13]. Once the autophagosomal membrane has fully
50 surrounded the cargo, it is closed leading to the capture of the marked cargo in a double membrane
51 autophagosome[14].

52 One of first critical steps in selective autophagy is the recruitment of Atg9 vesicles by Atg11 to
53 autophagic cargo. Deletion of Atg11 in yeast was initially shown to block the recruitment of Atg9
54 to autophagy cargos highlighting the important role of Atg11 in recruiting membrane to cargo
55 during selective autophagy initiation[15]. Atg11 was later shown to be required for the recruitment
56 of Atg9 vesicles to cargo mimetic beads in vitro using biochemical reconstitution[9]. Following on
57 this work, Atg11 was shown to directly interact with the flexible N-terminus of Atg9 via two PLF
58 motifs[8]. More recently, truncations or mutations within the N-terminal domain of Atg11 have been
59 shown to lead to a loss in the interaction between Atg11 and Atg9 in yeast[16]. These studies all
60 point towards an essential role for Atg11 in the recruitment of membrane to cargos, specifically
61 through the interaction between Atg11 and Atg9. However, while mutation of both PLF motifs in
62 Atg9 led to a near complete loss in the interaction between Atg11 and Atg9, it did not fully prevent
63 the recruitment of Atg9 to selective autophagy cargos[8]. Furthermore, the mammalian analog of
64 Atg11, FIP200, can bind membranes directly, although the exact function of membrane binding
65 by FIP200 is unknown[17]. Given these observations, we wanted to test if Atg11 is capable of binding
66 membranes and whether this plays a role in selective autophagy.

67

68 # RESULTS

69 ## Atg11 binds autophagosomal membranes in a clustered manner

70 To test if Atg11 can bind membranes we first purified Atg11 and GFP-Atg11 using Freestyle 293
71 cells as a recombinant expression system (**Figure S1**). Size exclusion chromatography of Atg11
72 in buffer containing 300mM NaCl had a similar elution profile and estimated molecular weight to
73 previously published purifications of Atg11 from insect cells where it was shown to be a dimer in

solution (**Figure S1B**)[18]. Next, we tested the ability of Atg11 to bind different membranes. Autophagosomal membranes and Atg9 vesicles are known to be composed of an unusually high concentration of negatively charged lipids, including between 37% and 44% of the negatively charged phosphatidylinositol (PI)[9,19]. Previously we have shown that several autophagy proteins including Atg23 and Atg16 bind membranes generated from yeast polar lipids (YPL), which also contain a high concentration of negatively charged lipids[20,21]. Therefore, we first tested if Atg11 can bind giant unilamellar vesicles (GUVs) made from YPL or a lipid mixture designed to mimic the autophagosomal membrane composition (43.9% phosphatidylcholine (PC), 19% phosphatidylethanolamine (PE), 32% phosphatidylinositol (PI), 5% phosphatidylinositol-3-phosphate (PI3P), and 0.1% rhodamine PE (RhPE) (automix+PI3P))[19]. 5% PI3P was added at the expense of PI as autophagosomal membranes contain PI3P but the exact concentration is unknown. GFP-Atg11 showed robust binding to YPL GUVs but was unable to bind autophagosomal membrane GUVs (**Figure 1A and B**). Given that Atg9 vesicles are highly curved while GUVs are essentially flat relative to the size of Atg11, we next investigated if membrane curvature impacts the ability of Atg11 to bind membranes. For this we employed supported membrane templates (SMrT) that consist of an array of highly curved membrane tubes ranging from 20-60 nm in diameter and supported lipid bilayers (SLB) resting on a PEGylated glass coverslip[22,23]. The size of the SMrT nanotubes match the size of Atg9 vesicles that are reported to be 30-60 nm in diameter while SLBs are primarily flat membranes[10,24]. We made SMrT and SLBs containing 43.2% PC, 19% PE and either 37% PI alone (automix) or 32% PI with 5% PI3P (automix+PI3P). Interestingly, GFP-Atg11 bound autophagosomal-like membranes as discreet clusters (**Figure 1C**). The presence of PI3P in membranes enhanced GFP-Atg11 recruitment. Importantly, the quantification of the ratio of GFP to membrane fluorescence showed that Atg11 binding was 5-fold higher on

97 tubes (mean = 0.8 ± 0.25) than on SLB (mean = 0.16 ± 0.07) suggesting that Atg11 membrane
98 binding is curvature sensitive (**Figure 1D**). As an independent validation of membrane binding,
99 we also performed a floatation assay with automix and automix+PI3P liposomes. Atg11 migrated
100 to the top layer of the sucrose density gradient in the presence of 100 nm diameter but not 1 µm
101 diameter automix+PI3P liposomes further supporting the curvature sensitivity of Atg11 membrane
102 binding (**Figure S2A**). DLS analysis also demonstrated that Atg11 binding to 100 nm liposomes
103 increased the diameter of these vesicles from 107 nm to 260 nm suggesting that Atg11 may also
104 be able to tether automix+PI3P liposomes (**Figure S2B**). These results suggest that Atg11 can bind
105 autophagosomal-like membranes in a curvature dependent manner and that this binding is
106 enhanced by the presence of PI3P.

107

108 The N-terminal (amino acids 1-646) and C-terminal (amino acids 700-1178) regions of Atg11 can
109 be purified using *E. coli* as a recombinant expression system[18]. Structure prediction of the N-
110 terminal region of Atg11 (Atg11-Nterm) using AlphaFold 3 demonstrates that it forms a helical
111 dimer with a structure that is similar to the N-terminal domain of FIP200 except that it is predicted
112 to form a Z shaped dimer instead of a C shaped dimer (**Figure S3A**)[25,26]. The C-terminal region of
113 Atg11 (Atg11-Cterm) contains a long coiled-coil domain, connected by linker regions to the Claw
114 domain that binds SARs[27,28]. We purified GFP-tagged Atg11-Nterm and -Cterm and analyzed
115 their membrane binding abilities using SMrT and SLBs (**Figure 1E**). Quantitative fluorescence
116 microscopy showed that Atg11-Nterm had significantly higher membrane binding than Atg11-
117 Cterm suggesting that the N-terminal region of Atg11 contains the primary membrane binding
118 region of Atg11 (**Figure 1F**). Moreover, unlike the full-length protein, Atg11-Nterm did not
119 cluster on membranes and instead bound both membrane tubes and SLBs in a diffuse manner

120 suggesting that membrane binding and clustering of Atg11 on membranes requires multiple
121 regions of Atg11.

122

123 Atg11 contains an amphipathic helix required for membrane binding

124 Sequence and structural analysis of the Atg11-Nterm revealed that it contains a predicted
125 amphipathic helix spanning residues 612-646, with the highest hydrophobic moment (μH=0.546)
126 occurring between residues 626 and 643 (**Figure 2A**). Amphipathic helices are known to mediate
127 curvature- and charge-dependent membrane binding[29,30]. Importantly, this region in the predicted
128 Atg11-Nterm structure has low and very low pLDDT scores, indicating that it is likely not in the
129 correct conformation in the structure prediction. This suggests that this helix may instead be
130 available for membrane binding (**Figure S3B**). Deletion of amino acids 612-646 from the Atg11-
131 Nterm sequence and rerunning the AlphaFold3 prediction did not alter the overall dimer structure
132 further suggesting that the predicted amphipathic helix is not required for formation of the Atg11-
133 Nterm dimer structure (**Figure S3C**). We therefore deleted the predicted amphipathic helix in
134 Atg11-Nterm (Atg11-Nterm$^{\Delta 612\text{-}646}$) and purified it using *E. coli* as a recombinant expression
135 system. We compared the elution profile of Atg11-Nterm$^{\Delta 612\text{-}646}$ from size exclusion
136 chromatography with that of Atg11-Nterm to verify that deletion of this helix did not disrupt the
137 overall shape of the protein (**Figure S3D**). The ability of GFP-Atg11-Nterm$^{\Delta 612\text{-}646}$ to bind
138 membrane tubes was tested using SMrT (**Figure 2B**). Comparison of GFP to membrane
139 fluorescence ratios revealed that Atg11-Nterm$^{\Delta 612\text{-}646}$ had 3-fold lower binding to membrane tubes
140 than Atg11-Nterm (**Figure 2C**). Together these results suggest that Atg11 binds autophagosomal-
141 like membranes in a curvature-dependent manner primarily via an amphipathic helix between

142 amino acids 612-646.

143

144 To determine if the amphipathic helix of Atg11 is required for selective autophagy in cells we
145 monitored the selective autophagy of mitochondria (mitophagy) using the established OM45-GFP
146 assay[31]. In this assay, the outer mitochondrial membrane (OMM) protein OM45 contains a C-
147 terminal GFP tag. Once OM45-GFP is delivered to the vacuole during mitophagy, OM45 is rapidly
148 degraded resulting in the production of free GFP. Deletion of the amphipathic helix of Atg11
149 resulted in a kinetic delay in mitophagy with a significant reduction in mitophagy at 2 hours which
150 recovered after 4 hours (**Figure 2D and E**). Importantly, deletion of amino acids 612-646 did not
151 alter the expression of Atg11 further suggesting that deletion of this helix did not destabilize Atg11
152 (**Figure 2F**). Atg32, an integral membrane protein residing in the OMM, functions as the SAR for
153 mitophagy in yeast[32,33]. In response to mitophagy inducing conditions, Atg32 clusters on the
154 surface of mitochondria (**Figure S4A**). Atg32 puncta co-localize with Atg8 and are eventually
155 delivered to the vacuole (**Figure S4B**). These Atg32 puncta therefore represent mitophagy
156 initiation sites[34]. We previously demonstrated that truncations and mutations of the third coiled-
157 coil domain of Atg11 resulted in a change in the clustering of Atg32 during mitophagy initiation
158 which suggested an important link between the morphology of Atg11 and Atg32 during mitophagy
159 initiation[27]. Therefore, we also tested to see if Atg11$^{\Delta 612\text{-}646}$ altered the formation of Atg32 puncta.
160 RFP-Atg32 puncta formed and co-localized with 2xGFP-Atg11 and 2xGFP-Atg11$^{\Delta 612\text{-}646}$
161 suggesting that deletion of the amphipathic helix did not affect recruitment of Atg11 during
162 mitophagy (**Figure S4C**). To further test if Atg11$^{\Delta 612\text{-}646}$ altered the kinetics of mitophagy
163 initiation, we monitored the formation of GFP-Atg32 puncta, in response to nitrogen-starvation,
164 in real-time using the temperature- and flow rate- controlled FCS2 chamber (**Figure 2G**). We

165 found that, at 28 minutes post starvation, 50% of cells expressing WT Atg11 had at least one GFP-
166 Atg32 punctum (**Figure 2H, Supplemental Movie 1)**. Strikingly, only 20% of cells expressing
167 Atg11$^{\Delta 612\text{-}646}$ had at least one GFP-Atg32 puncta at 28 minutes post starvation (**Supplemental**
168 **Movie 2**). This suggests that the deletion of the predicted amphipathic helix in Atg11 led to a delay
169 in the kinetics of mitophagy initiation.

170

171 Atg11 forms clusters in solution

172 Formation of autophagy protein condensates have been proposed to enhance weak protein
173 interactions, direct the formation of protein-complexes, and play a role in the overall organization
174 of autophagy initiation sites[35,36]. We observed that GFP-Atg11 clustered on membrane tubes and
175 SLBs which prompted us to investigate if Atg11 may cluster in solution or if the clustering of
176 Atg11 is induced by membrane binding. GFP-Atg11 was purified in the presence of 300 mM NaCl
177 as this was previously reported to allow for soluble full-length Atg11[9,18]. Therefore, we monitored
178 1 μM GFP-Atg11 by confocal microscopy to determine if it formed puncta, which would indicate
179 clustering of Atg11 (**Figure 3A**). We found that while GFP-Atg11 appeared largely diffuse at 300
180 mM NaCl, it formed puncta when the NaCl concentration was reduced to 150 mM or less (**Figure**
181 **3A and B**). We next asked if the formation of these puncta was dependent on the concentration of
182 Atg11. We diluted GFP-Atg11 to concentrations from 0.05 μM to 5.0 μM into buffer with a final
183 concentration of 150 mM NaCl (**Figure 3C**). We observed that increasing the concentration of
184 Atg11 increased the number of Atg11 puncta indicating that Atg11 clustering is both salt and
185 concentration dependent (**Figure 3D**). The puncta we observed were not liquid-like condensates
186 as they are not entirely circular, nor did we observe the fusion of any puncta. This is in contrast to

187 the non-selective autophagy initiation complex which was shown to undergo liquid-liquid phase
188 separation[36]. It is possible that diluting Atg11 into 150 mM NaCl resulted in an irreversible
189 aggregation event. Therefore, to test if the formation of Atg11 puncta was reversible, we first
190 generated Atg11 puncta in 150 mM NaCl, and then increased the NaCl concentration to 300 mM
191 by mixing the 1 μM Atg11 in 150 mM NaCl with 1 μM of Atg11 in 450 mM NaCl (**Figure 3E**).
192 After the samples were mixed, we saw a near complete loss in the formation of Atg11 puncta
193 suggesting that these Atg11 clustering events are reversible in solution (**Figure 3F**). We next
194 wanted to determine whether Atg11-Nterm or Atg11-Cterm could undergo similar clustering
195 events as full-length Atg11 in solution. Therefore, we diluted GFP-Atg11, GFP-Atg11-Nterm and
196 GFP-Atg11-Cterm into buffer containing 150 mM NaCl. While GFP-Atg11 formed puncta at 1
197 μM in 150 mM NaCl, neither the Nterm nor Cterm regions of Atg11 formed puncta at 1 μM in
198 150 mM NaCl, suggesting that the ability of Atg11 to cluster is a property of the full-length protein
199 (**Figure 3G**). This data demonstrates that full-length Atg11 can form reversible puncta that are salt
200 and concentration dependent while the Nterm and Cterm regions of Atg11 are unable to form
201 puncta. This is consistent with our membrane binding observations in **Figure 1** where full-length
202 Atg11 bound to membranes in a clustered fashion while the Nterm and Cterm regions of Atg11
203 bound membranes in a diffuse manner.

204

205 A novel fluorescence-microscopy-based assay to study membrane tethering

206 We have demonstrated that Atg11 can bind membranes in a clustered manner via a predicted
207 amphipathic helix and that a loss of this helix leads to a delay in the formation of Atg32 puncta
208 and the onset of mitophagy in yeast. Since Atg11 binding to Atg32 is critical for the recruitment

209 of Atg9 vesicles to mitochondria in yeast, we wanted to determine if the interaction between Atg32
210 and Atg11 could result in the recruitment of autophagosomal-like vesicles to sites of mitophagy
211 using biochemical reconstitution[7]. Atg9 vesicle recruitment by the Atg32-Atg11 complex is a
212 process in which highly curved autophagy precursor vesicles are recruited to the relatively flat
213 outer mitochondrial membrane. This recruitment results in a heterotypic membrane tethering event
214 between flat and curved membranes containing different lipid compositions. However, while much
215 work has focused on the establishment of methods to reconstitute and study selective autophagy
216 in vitro, these efforts have focused on protein-based cargos or cargo mimetics including Sepharose
217 or agarose beads[9,37-39]. As such, we searched the membrane trafficking literature to identify a
218 method that would be suitable for reconstituting and monitoring heterotypic tethering in vitro but
219 we found no established methods that were suitable for our studies. Therefore, we next established
220 and validated a new method to study heterotypic membrane tethering which we have termed GUV
221 and Liposome Tethering (GLT) that is derived from our recent work on Atg23[20]. We believe that
222 this assay will be broadly useful for studying organelle selective autophagy in vitro in addition to
223 membrane tethering.

224

225 To establish an assay to study heterotopic membrane tethering in vitro we added liposomes to
226 GUVs labeled with different fluorophores. We hypothesized that in the absence of a tethering
227 protein, the liposomes would diffuse around the GUV while in the presence of a tethering protein
228 the liposomes would be anchored to the GUV (**Figure 4A**). We reasoned that the large size of
229 GUVs (typically 1 to 100 µm in diameter) would allow us to directly visualize liposomes tethered
230 on the GUV surface, thus eliminating ambiguities arising due to aggregation of liposomes and/or
231 protein. Liposomes can be extruded or sonicated to achieve a diameter ranging from 60 nm to 1

232 μm which would also allow for the analysis of curvature-dependent tethering. Lastly, GUVs would
233 allow us to observe if a fluorescently tagged protein also localizes at tethering sites further adding
234 to the applications of such an assay.

235

236 To initially test the feasibility of GLT we engineered an artificial membrane tether by fusing the
237 monomeric PI3P-binding EEA1 $FYVE_{1337-1411}$ with GST (GST-FYVE)[40]. Since GST dimerizes,
238 this generates a stable dimer of EEA1 $FYVE_{1337-1411}$ with two PI3P binding sites in a single protein
239 complex. Similarly engineered tethers generated by linking membrane binding domains to GST
240 have been shown to facilitate clustering of small liposomes[41]. GUVs containing PI3P were first
241 incubated with GST-FYVE, followed by incubation with 400 nm liposomes containing an identical
242 lipid composition to the GUVs except for a different fluorophore for detection. GUVs mixed with
243 PI3P-liposomes alone or with the addition of purified GST showed no co-localization between
244 GUVs and liposomes (**Figure 4B and C**). In contrast, addition of PI3P-liposomes to GUVs pre-
245 incubated with 1 μM GST-FYVE showed robust recruitment of liposomes to GUVs as illustrated
246 by fluorescence intensity traces along the surface of a GUV in the liposome fluorescence channel
247 (**Figure 4D**). Comparison of liposome fluorescence per micron calculated along the surface of
248 GUVs further showed that tethering of liposomes to GUVs only occurred in the presence of GST-
249 FYVE (**Figure 4E**). To further demonstrate that membrane tethering is directly mediated by the
250 membrane-binding FYVE domains, we generated a GST-GFP-FYVE construct. Repeating the
251 GLT assay with GST-GFP-FYVE showed that the protein coated GUVs and tethered liposomes
252 (**Figure 4F**). In addition, fluorescence intensity traces revealed that areas with tethered liposomes
253 showed increased intensity of GST-GFP-FYVE demonstrating that protein is localized to tethering
254 sites (**Figure 4G**). Together these results validate the GLT assay for the study of membrane

255 tethering in vitro and highlight the applicability of this technique to monitor protein colocalization
256 with tethering events.

257

258 GLT demonstrates autophagosomal-like liposome tethering by the Atg32-
259 Atg11 complex

260 Having established that GLT can be used to monitor membrane tethering in vitro, we asked if the
261 ability of Atg11 to bind membranes allows for the tethering of autophagosomal-like liposomes on
262 the surface of mitochondrial membranes. To do this, we made GUVs containing a lipid
263 composition similar to the OMM (OMM-GUVs)[42]. GFP-Atg11 alone was unable to bind these
264 OMM-GUVs further highlighting that Atg11 is not a broad membrane binding protein (**Figure**
265 **S5A**). Next, we displayed the cytosolic domain of the mitophagy SAR Atg32 (1-381), which
266 contains the Atg11 binding region, fused to an N-terminal GFP and a C-terminal 10xHistidine tag,
267 on OMM-GUVs (**Figure S5B**)[34]. GUVs included 5 mol% of DGSNi^{2+}NTA to recruit of the
268 cytosolic domain of GFP-Atg32$_{1-381}$. To monitor if Atg11 can bind to these Atg32-displaying
269 OMM-GUVs, we labeled purified Atg11 with Alexa Flour 594. Atg11 was recruited on GFP-
270 Atg32$_{1-381}$ bound GUVs. In contrast, no Atg11 recruitment occurred on GUVs displaying
271 6xHistidine tagged GFP (**Figure S5C)**, demonstrating that Atg11 requires Atg32 for its
272 recruitment to the surface of OMM-GUVs (**Figure S5D**). To test if the Atg32-Atg11 complex
273 could tether autophagosomal-like liposomes, we added sonicated automix+PI3P liposomes,
274 mimicking the lipid composition and size of Atg9 vesicles (30 nm diameter), to GFP-Atg32$_{1-381}$
275 OMM-GUVs in the presence and absence of Atg11 (**Figure 5A**). Automix+PI3P liposomes were
276 recruited to Atg32$_{1-381}$ bound GUVs only in the presence of Atg11 (**Figure 5B-E**). Fluorescence

277 intensity traces along the GUVs further confirm that peaks of liposome fluorescence correspond
278 with peaks of GFP-Atg32$_{1-381}$ fluorescence and were only seen in presence of Atg11 (**Figure 5C**
279 and **D**). Interestingly, tethered automix+PI3P liposomes appeared punctate on the GUV and these
280 overlap with peaks of Atg32 fluorescence, suggesting that Atg11 may be able to cluster Atg32 and
281 liposomes (**Figure 5C**). In comparison, GFP-Atg32 fluorescence was uniform in the absence of
282 Atg11 (**Figure 5D**). While Atg11 robustly tethered 30 nm automix+PI3P liposomes to Atg32
283 OMM-GUVs, the ability of Atg11 to recruit larger automix+PI3P liposomes (1 μm diameter) was
284 drastically reduced (**Figure 5F** and **G**). This is in agreement with our results on SMrT showing
285 that automix+PI3P membrane binding by Atg11 occurred in a curvature-dependent manner.

286

287 We hypothesized that using YPL could override the need for curvature as Atg11 was able to bind
288 GUVs containing YPL but not automix+PI3P GUVs (**Figure 1A**). This may be due to the
289 heterogeneity of lipids present in YPL which could lead to packing defects similar to what would
290 be expected for more highly curved vesicles[48]. To test if Atg11 was also able to tether larger YPL
291 liposomes to GUVs, we performed the GLT assay with 400 nm YPL liposomes and GFP-Atg32$_{1-}$
292 $_{381}$ bound GUVs in the presence and absence of Atg11 (**Figure S6A**). As expected, YPL liposomes
293 were tethered on GUVs only in the presence of Atg11 (**Figure S6B** and **E**) and the tethered
294 liposomes colocalized with regions of higher Atg32 fluorescence (**Figure S6C** and **D**). We again
295 observed that GFP-Atg32 was uniform on the surface of the GUV in the absence of Atg11 but
296 concentrated into distinct peaks when Atg11 was present.

297

298 **The N-terminal region of Atg11 is critical for membrane tethering**

299 Our results till now show that Atg11 binds membranes via a putative amphipathic helix located in
300 its N-terminus and that it can self-associate to form puncta. Additionally, the interaction between
301 Atg11 and Atg32 leads to membrane tethering in vitro. Therefore, to test if the Atg11-Nterm
302 contributes to tethering of autophagosomal-like liposomes, we carried out GLT using GFP-Atg32$_{1-}$
303 $_{381}$ bound OMM-GUVs and automix+PI3P liposomes with Atg11 alone and Atg11 mixed with 20-
304 fold molar excess of Atg11-Nterm (**Figure 6A**). We reasoned that excess Atg11-Nterm would
305 compete with the full-length Atg11 and inhibit tethering of automix+PI3P to GUVs. As a control
306 we also carried out the GLT assay using Atg11 mixed with 20-fold molar excess of GST.
307 Quantification of the fluorescence intensity of liposomes normalized to that of GFP-Atg32$_{1-381}$
308 showed that the addition of excess Atg11-Nterm led to a near complete block in automix+PI3P
309 liposome tethering (**Figure 6B**). Atg11 mixed with an excess of GST had only a modest reduction
310 in the tethering of automix+PI3P liposomes. This lends further support to the idea that
311 autophagosomal-like liposome tethering by Atg11 occurs via membrane binding by the N-terminal
312 region of Atg11.

313

314 Next, we compared the liposome tethering abilities of full-length Atg11 with that of the Atg11-
315 Nterm. Full-length Atg11 was mixed with GFP-Atg32$_{1-381}$ bound OMM-GUVs and subsequently
316 incubated with automix+PI3P liposomes (**Figure 6C**). Because the Atg32 binding interface lies at
317 the C-terminus of Atg11, we directly recruited Atg11-Nterm to NTA-containing mitochondrial
318 GUVs and subsequently added automix+PI3P liposomes. GUV recruited Atg11-Nterm was also
319 able to tether liposomes further supporting the role of the Atg11-Nterm in membrane binding and
320 tethering. Intriguingly, while liposomes tethered via full-length Atg11 showed a punctate
321 distribution, liposomes tethered via Atg11-Nterm uniformly coated the GUVs (**Figure 6C** zoom

322 image). Fluorescence intensity traces along the GUVs revealed that automix+PI3P liposomes
323 tethered by full-length Atg11 showed discreet peaks. In comparison, liposomes tethered via Atg11-
324 Nterm had a lower and more uniformly distributed intensity (**Figure 6C**). Distribution of
325 liposomes can be quantitated by comparing the coefficient of variance (COV) of liposome
326 fluorescence, calculated as mean by standard deviation, which measures the extent of clustering.
327 We found that the COV for Atg11-Nterm is significantly lower than the COV for full-length Atg11
328 (**Figure 6D)**, suggesting that while OMM-GUV bound Atg11-Nterm alone can tether
329 autophagosomal-like liposomes, it fails to cluster these liposomes. Importantly, clustering of
330 liposomes by Atg11 led to more efficient tethering of automix+PI3P liposomes as the liposome
331 fluorescence per micron calculated along the surface of GUVs was significantly higher for full-
332 length Atg11 than Atg11-Nterm (**Figure 6E**).

333

334 DISCUSSION

335 Our results demonstrate for the first time that Atg11 can bind highly curved membranes containing
336 an autophagosomal-like lipid composition. Intriguingly, we observed that Atg11 membrane
337 binding occurred in a punctate manner and that this clustering of Atg11 could be recapitulated in
338 the absence of membrane. We also demonstrated that a putative amphipathic helix in the N-
339 terminal region of Atg11 is the main membrane binding region and that a deletion of this helix
340 results in a delay in mitophagy in yeast. To further explore the role of Atg11 membrane binding,
341 we developed a novel method, termed GLT, to reconstitute membrane tethering in vitro which we
342 believe will be broadly useful for studying organelle selective autophagy in vitro. We validated
343 this method using an established model tether, demonstrating the general approach and usefulness
344 of the assay. Lastly, using GLT we demonstrated that the interaction between Atg32 and Atg11

345 can lead to the recruitment of autophagosomal-like liposomes to OMM-GUVs. The recruitment of
346 liposomes to GUVs by Atg11 occurred in a punctate manner which required full length Atg11 for
347 liposome clustering as Atg11-Nterm was able to recruit liposomes but was unable to cluster them.

348

349 Our work demonstrating that Atg11 can directly interact with membranes is in contrast to a
350 previous study showing that Atg11 was unable to bind membranes[7]. However, two key differences
351 could account for the observed discrepancy in the membrane binding abilities of Atg11. First, we
352 recombinantly expressed and purified Atg11 from Freestyle 293 cells where it appears to be a
353 dimer as opposed to recombinant expression and purification from *E. coli* where Atg11 was
354 reported to be a monomer (**Figure S1B**). Second, we used liposomes containing YPL and
355 autophagosomal-like lipid compositions. Both of these mixtures contain approximately 42%
356 negatively charged lipids. In contrast, monomeric Atg11 was previously shown to be unable to
357 bind liposomes composed of 60% POPC, 20% Cholesterol, 10% POPE and 10% POPS which
358 contain only 10% negatively charged lipids[7]. Therefore, it is possible that Atg11 membrane
359 binding requires a high negative charge which is consistent with the composition of the
360 autophagosomal membrane[19].

361

362 We have previously demonstrated that another member of the autophagy initiation machinery,
363 Atg13, was able to bind liposomes containing 42.5% negatively charged lipids but not to liposomes
364 containing 19% negatively charged lipids[20,43]. We have also now shown that Atg11 can bind to
365 YPL or membranes containing greater than 37% negatively charged lipids. This begins to point
366 towards a possible common mechanism for membrane binding by some autophagy proteins,

367 wherein these proteins can preferentially bind to membranes with a high concentration of
368 negatively charged lipids that are present in the autophagosomal membrane but that are not present
369 in the cargo membrane during organelle selective autophagy. This may play an important role in
370 organizing autophagy proteins on the side of the autophagosomal membrane during
371 autophagosome expansion.

372

373 The interaction between Atg9 and Atg11 was previously shown to be only partially required for
374 the recruitment of Atg9 vesicles to cargo in yeast[8]. Our results support this in that Atg11 can bind
375 to autophagosomal-like membranes directly and tether them to OMM-GUVs in vitro in the absence
376 of Atg9. Given these results it is possible that mitochondrial-recruited Atg11 may participate in
377 the tethering of Atg9 vesicles to mitochondria by binding to both Atg9 and the autophagosomal
378 membrane directly. We also observed that deletion of the membrane binding helix of Atg11 results
379 in a delay in mitophagy initiation. Therefore, we propose that Atg11 membrane binding aids Atg9
380 vesicle recruitment which is essential for rapid initiation of selective autophagy (**Figure 7**). Atg11
381 could aid Atg9 vesicle recruitment in several possible ways. First, membrane association via the
382 amphipathic helix may work synergistically with the interaction between Atg11 and Atg9 thereby
383 enhancing the recruitment of Atg9 vesicles to selective autophagy initiation sites. Second, Atg9
384 localizes to various compartments along the vesicular transport pathway. Thus, co-incident
385 interactions of Atg11 with negatively charged, curved membranes and the presence of Atg9 could
386 facilitate its selective binding to Atg9 vesicles specifically at autophagy initiation sites. Third,
387 given the clustering properties of Atg11 and its important role in organizing Atg32 puncta, Atg11
388 membrane binding and clustering may also help to organize Atg9 vesicles on the surface of

389 mitochondria to enhance the efficiency of mitophagy[27]. However, which of these possibilities is
390 correct will need to be further explored in subsequent work.

391

392 Lastly, we also demonstrated the broad usefulness of GLT to quantitatively analyze membrane
393 tethering in vitro and monitor the localization of protein components at sites of tethering. This
394 assay can be easily applied to study homotypic or heterotypic tethering events making it ideal to
395 reconstitute and examine tethering occurring at organelle contact sites, vesicle trafficking, and
396 autophagosome biogenesis. We believe that GLT will serve as an excellent starting point for
397 reconstitution of organelle selective autophagy in vitro and enable future studies to explore the
398 complicated mechanisms of organelle selective autophagy.

399

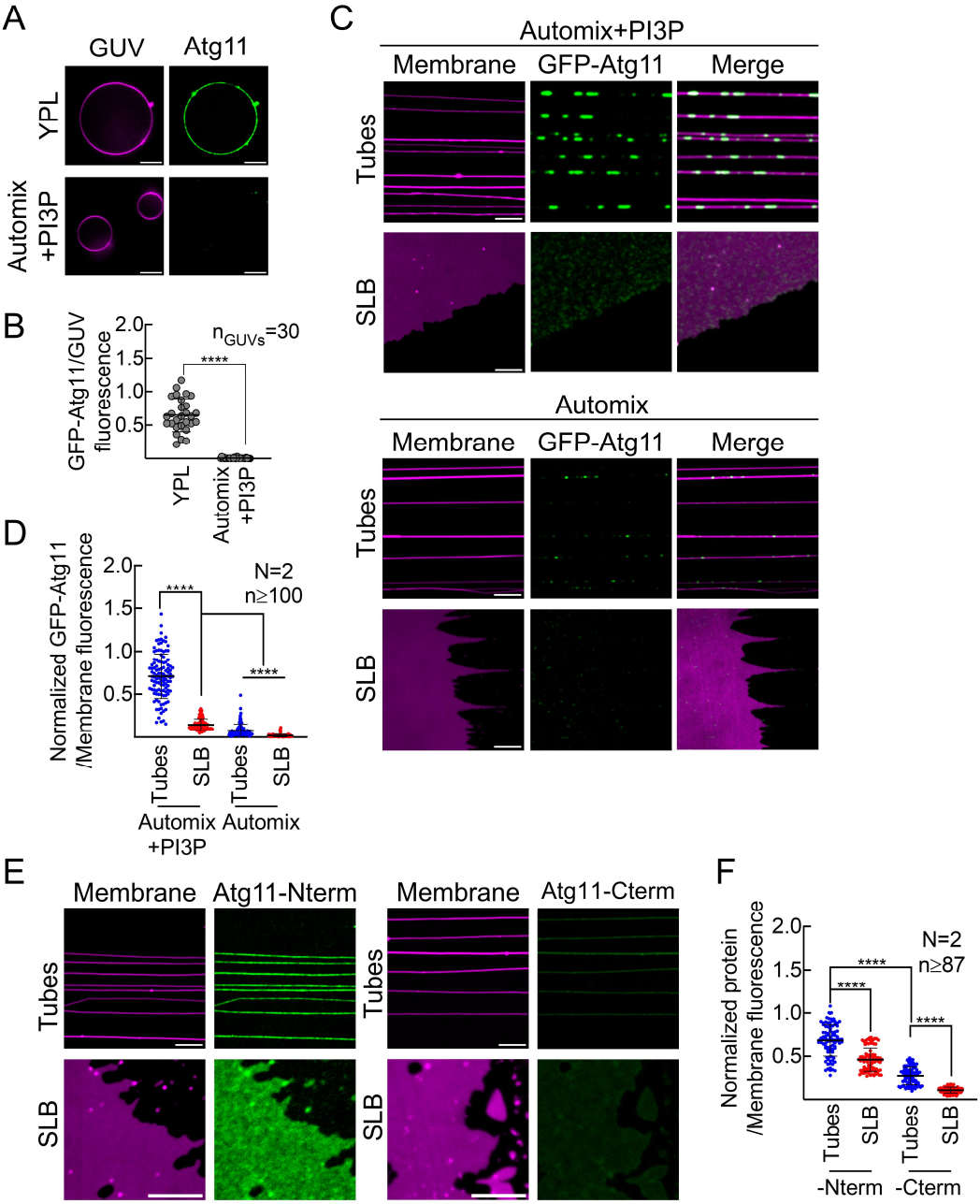

Figure 1. Atg11 binds curved autophagosomal-like membranes. (**A**) Representative images showing binding of full-length GFP-Atg11 on GUVs containing yeast polar lipids (YPL, top panel) and autophagosomal-like membrane with PI3P (automix+PI3P) (bottom). Scale bar=10µm. (**B**) Quantification showing mean ± SD of GFP-Atg11 fluorescence normalized to membrane fluorescence from GUVs made of YPL and automix+PI3P. A total of 30 YPL and automix+PI3P GUVs each were analyzed (n=30). **** indicates $p<0.0001$ calculated using the non-parametric Mann-Whitney's test. (**C**) Representative images showing binding of GFP-Atg11 on an array of curved tubes and flat supported lipid bilayers (SLB). Membranes (magenta) are made of autophagosomal-like membrane with PI3P (Automix+PI3P, left panel) and without PI3P

410 (Automix, right panel). Scale bar=5µm. (**D**) Quantification of GFP-Atg11 fluorescence normalized
411 to the membrane fluorescence from tubes and SLB made with automix+PI3P and automix. A total
412 100 tubes or 2 to 4um^2 individual patches of SLB (n=100) were analyzed across two independent
413 repeats (N=2). Data represent mean ± SD. **** indicates p<0.0001 calculated using one-way
414 ANOVA. (**E**) Representative fluorescence micrographs showing the binding of GFP-Atg11-Nterm
415 and GFP-Atg11-Cterm on an array of tubes and SLB made of autophagosomal lipids with PI3P.
416 Scale bar=5µm. (**F**) Quantification of GFP-Atg11-Nterm or -Cterm normalized to membrane
417 fluorescence for tubes and SLB. A total of 87 tubes or 2 to 4um^2 individual patches of SLB (n=100)
418 were analyzed across two independent repeats (N=2). Data represent mean ± SD. **** indicates
419 p<0.0001 calculated using Kruskal-Wallis test. Autophagosomal-like membranes with PI3P
420 (automix+PI3P) were made of 43.2mol% PC, 19mol% PE, 32mol% PI, 5mol% PI3P with
421 0.1mol% RhPE. Autophagosomal-like membranes without PI3P (automix) were made similarly
422 except for the omission of PI3P and increase of PI to 37mol%.

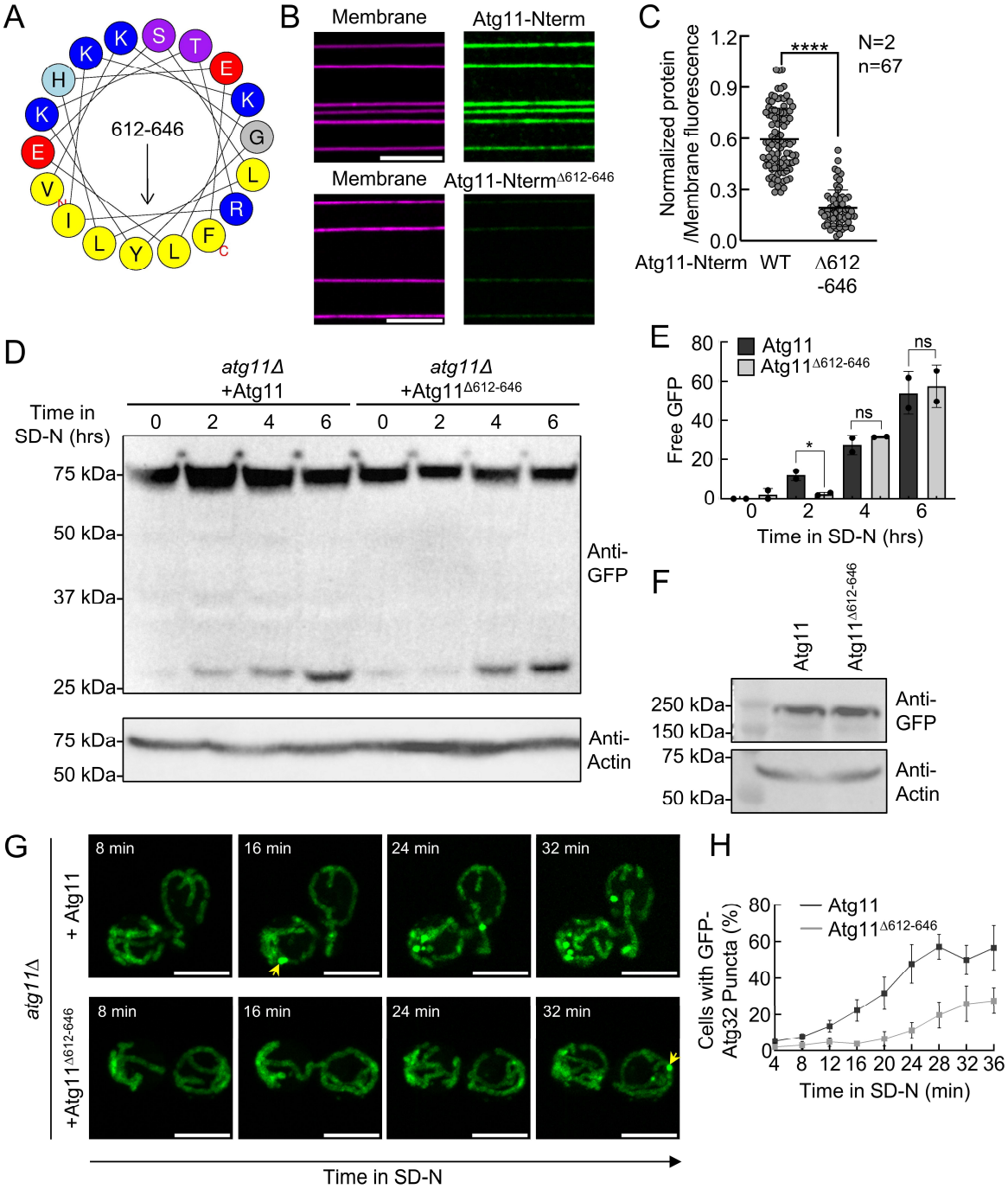

Figure 2. A putative amphipathic helix mediates autophagosomal membrane binding by Atg11 and contributes to mitophagy. (**A**) Helical wheel representation of the predicted amphipathic helix in Atg11-Nterm. (**B**) Representative images showing GFP-Atg11-Nterm or GFP-Atg11-Nterm$^{\Delta 612-646}$ binding on membrane tubes. Scale bar=5μm. **C**) Quantification of GFP-Atg11-Nterm or GFP-Atg11-Nterm$^{\Delta 612-646}$ fluorescence normalized by membrane fluorescence

429 from **B**. Membrane tubes contained 43.2% PC, 19% PE, 32% PI, 5% PI3P with 0.1mol% RhPE
430 (automix+PI3P). Data represent mean ± SD of 67 tubes (n=67) analyzed across two independent
431 repeats (N=2). **** indicates p<0.0001 calculated using the non-parametric Mann-Whitney's test.
432 (**D**) *Atg11*Δ cells transformed with Atg11 or Atg11$^{\Delta 612\text{-}646}$ were grown in media containing lactate
433 and shifted to nitrogen starvation media (SD-N) to induce mitophagy. Western blot showing
434 OM45-GFP at 0, 2, 4 and 6 hours after nitrogen starvation. Actin was used as a loading control.
435 (**E**) Quantification of the background subtracted free GFP band at 0, 2, 4 and 6 hours after nitrogen
436 starvation. Data represent mean ± SD from two independent repeats. * indicates p=0.0436. ns is
437 not significant as analyzed using Student t-test. **(F)** Western blot showing the expression of
438 2xGFP-Atg11 and 2xGFP-Atg11$^{\Delta 612\text{-}646}$. (**G**) Timelapse fluorescence images showing *Atg11*Δ
439 cells expressing GFP-Atg32 with Atg11 (top panel) or Atg11$^{\Delta 612\text{-}646}$ (bottom panel). Cells grown
440 in nutrient rich (SMD) media were attached to a concanavalin A-treated coverslip, assembled in a
441 flow cell maintained at 30°C. Nitrogen-starvation medium (SD-N) was introduced under
442 controlled laminar flow, and time-lapse images were acquired three minutes after the flow
443 initiation. Images were captured at 4 minutes interval. Yellow arrowheads indicate the onset of
444 GFP-Atg32 puncta formation. Scale bar=5µm. (**H**) Quantification of G showing percent of cells
445 with at least one GFP-Atg32 puncta. A total of 102 cells for Atg11 and 109 cells for Atg11$^{\Delta 612\text{-}646}$
446 from four different fields were analyzed. Data points represent mean ± SD of percent cells with at
447 least one GFP-Atg32 puncta.

448

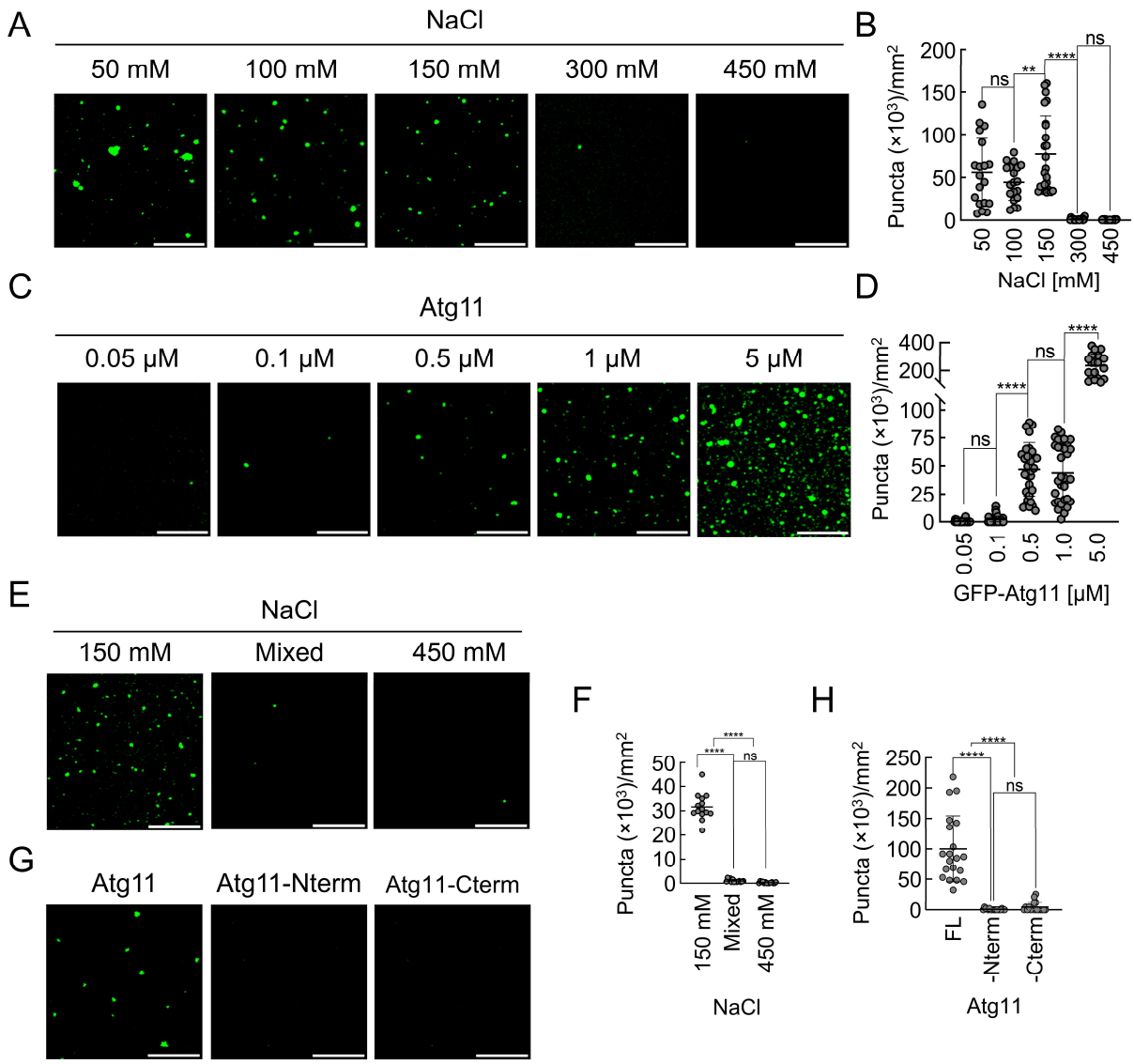

Figure 3. Atg11 self-associates in a salt and concentration dependent manner. Purified GFP-Atg11 was diluted into different buffers and imaged by confocal microscopy to detect the presence of Atg11 puncta. (**A**) GFP-Atg11 puncta formation at 1uM protein concentration in different NaCl concentrations (as indicated). Scale bar=5μm. (**B**) Quantification of A. (**C**) GFP-Atg11 puncta formation in 150 mM NaCl at different protein concentrations (as indicated). Scale bar=5μm. (**D**) Quantification of C. (**E**) GFP-Atg11 was diluted to 1 μM in 150 mM or 450 mM NaCl, then imaged. Samples were mixed to produce 300 mM NaCl at 1 μM protein concentration. (**F**) Quantification of E. (**G**) Representative images of clustering observed when GFP-Atg11 constructs (FL, Atg11-Nterm or Atg11-Cterm) were diluted to 1 μM in 150 mM NaCl and imaged as before. (**H**) Quantification of clustering observed when GFP-Atg11 constructs (FL, Atg11-Nterm or Atg11-Cterm) were diluted to 1 μM in 150 mM NaCl and imaged as before. Each experiment was conducted in 3 independent repeats, with 7 images acquired at each repeat, amounting to a total area of 30492 μm^2 per repeat. Puncta analyzed varied from ~30 to ~19,000,

463 depending on the group. The number of puncta was normalized to the area imaged, yielding
464 particles per mm^2. The data are presented as means, with error bars indicating standard deviation.
465 Groups were compared using a one-way ANOVA test with Tukey's correction for multiple
466 comparisons. * $p< 0.05$, ** $p<0.01$, *** $p<0.001$, **** $p<0.0001$, ns is not significant.

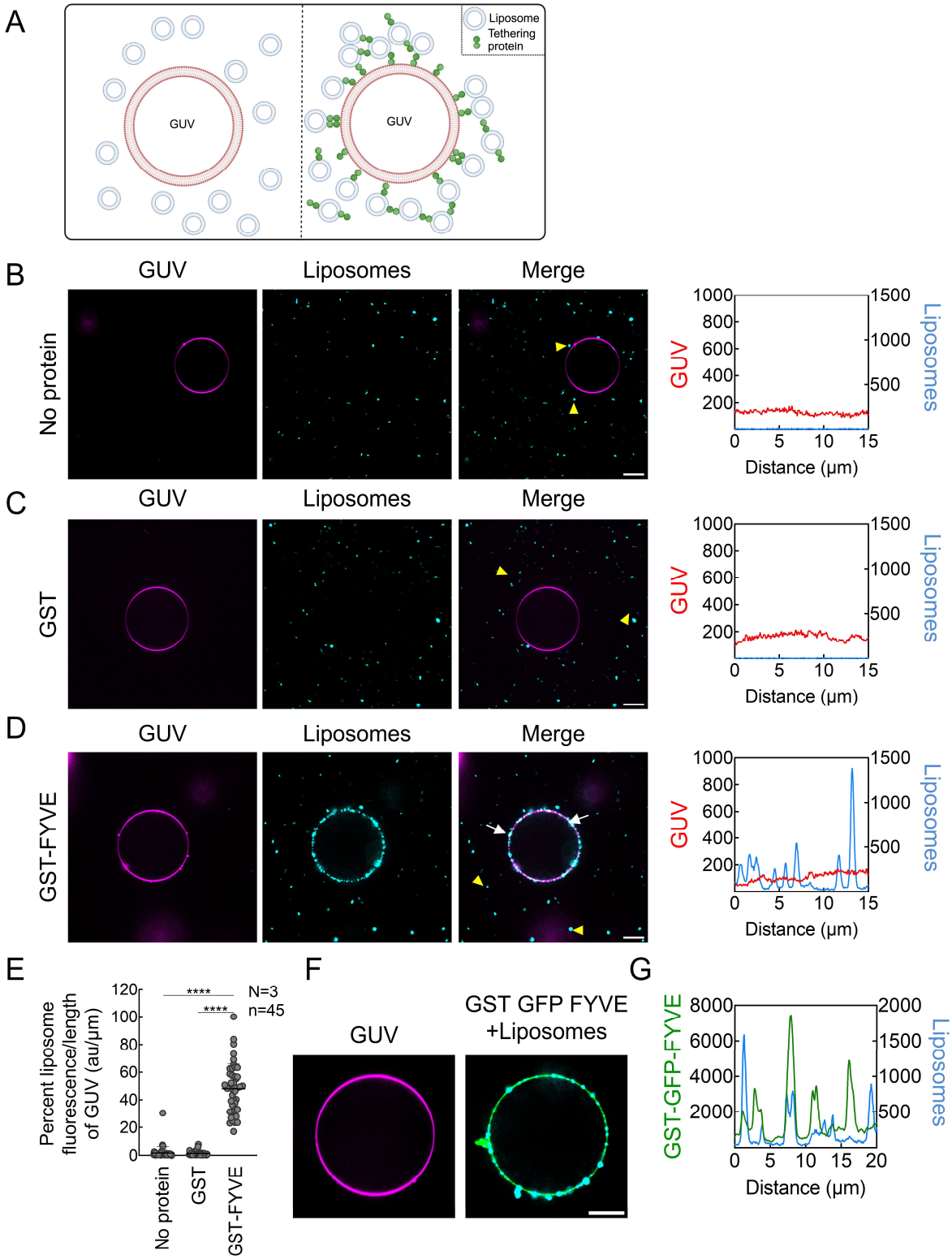

Figure 4. Validation of GUV Liposome Tethering (GLT) Assay (**A**) Schematic showing fluorescence microscopy-based GUV liposome tethering (GLT) assay. GUVs and liposomes containing different fluorophores are mixed with candidate tethering protein capable of binding

both membranes. Tethering is visualized by the co-localization of liposomes and GUVs in presence of a tethering protein. Representative images showing 400 nm-extruded liposomes mixed with GUVs (**B**), GUVs and GST (**C**), or GUVs and GST-FYVE (**D**). Merged images show yellow arrowheads indicating free liposomes and white arrowheads indicating liposomes tethered to GUVs. Fluorescence intensity profiles for the GUV and liposome channels along the circumference of the GUV are shown to the right of each representative image. (**E**) Scatter plots showing the percent of liposome fluorescence per length of GUV normalized to the largest signal from B to D. The data are presented as means, with error bars indicating standard deviation. Data from 3 independent repeats (N=3) were pooled and analyzed using non-parametric Mann-Whitney's test. **** indicates $p<0.0001$. n indicates total number of GUVs analyzed for each condition. (**F**) Representative fluorescence images showing GUVs containing PI3P mixed with GST-GFP-FYVE followed by incubation with PI3P-containing liposomes. (**G**) Fluorescence intensity profiles for the liposome and protein fluorescence channels around the circumference of the GUV shown in F. GUVs were made with 74.9 mol% DOPC, 20 mol% DOPS, 5 mol% PI3P and 0.1 mol% rhodamine PE (RhPE). Liposomes were made with 74.9 mol% DOPC, 20 mol% DOPS, 5 mol% PI3P and 0.1 mol% of the fluorescent lipophilic dye DiD. Scale bar=10μm.

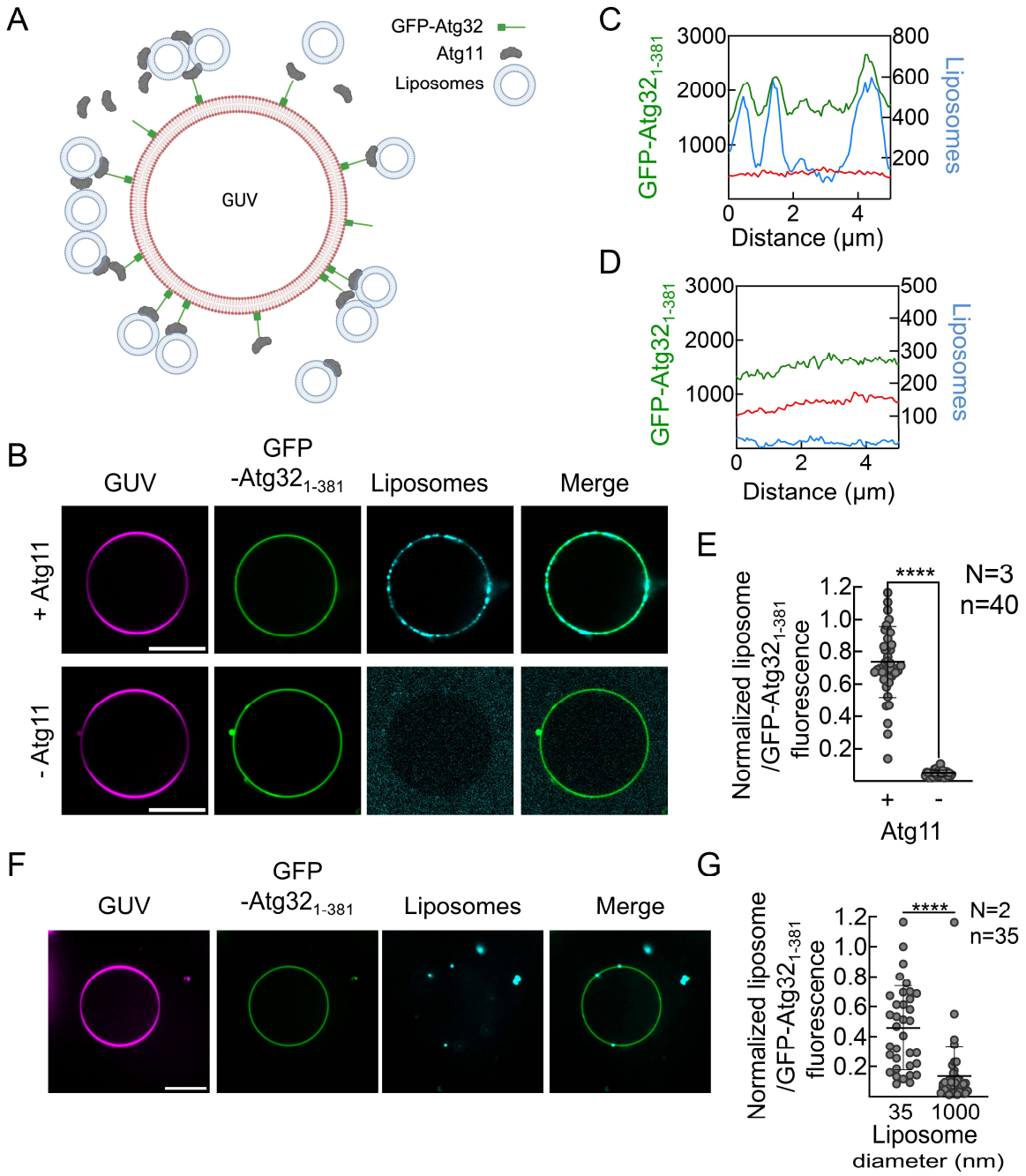

Figure 5. Atg11 and Atg32 coordinate to tether curved autophagosomal membranes to cargo mimetics. (**A**) Schematic showing tethering of autophagosomal membranes to mitochondrial mimetic GUV reconstituted using GLT assay. OMM GUVs containing mitochondrial lipids and DGS-Ni^{+2}NTA (5 mol%) displaying the cytosolic domain of Atg32 (His-GFP-Atg32$_{1-381}$) are used as a mitochondria mimic to recruit Atg11. 35nm-automix+PI3P liposomes are then added to reconstitute heterotypic tethering by the Atg32-Atg11 complex. (**B**) Representative fluorescence images of GLT with GUVs containing 5% mol DGS-Ni^{+2}NTA displaying His-GFP-Atg32$_{1-381}$

495 which were sequentially incubated with Atg11 and automix+PI3P liposomes (top panel) or
496 automix+PI3P liposomes alone (bottom panel). Scale bar=10µm. (**C**) Fluorescence intensity
497 profiles from a line drawn along the GUV in B (top panel) showing liposome and GFP-Atg32$_{1-381}$
498 fluorescence intensities along the GUV. (**D**) Fluorescence intensity profiles from a line drawn
499 along the GUV in B (bottom panel) showing liposome and GFP-Atg32$_{1-381}$ fluorescence intensities
500 along the GUV. (**E**) Quantification of the ratio of liposomes to GFP-Atg32$_{1-381}$ fluorescence from
501 B. Data are presented as means ± SD from 3 independent repeats (N=3). ****$p<0.0001$ analyzed
502 using Mann-Whitney's test. n indicates total number of GUVs analyzed per condition. ns indicates
503 not significant. (**F**) Representative image of a GUV containing 5% mol DGS-Ni^{+2}NTA displaying
504 His-GFP-Atg32$_{1-381}$ sequentially incubated with Atg11 and 1µm-automix+PI3P liposomes. (**G**)
505 Quantification of the ratio of liposomes to GFP-Atg32$_{1-381}$ fluorescence from F. Data are presented
506 as means ± SD from 2 independent repeats (N=2). n indicates the total number of GUVs analyzed
507 per condition. **** indicates $p<0.0001$ analyzed using non-parametric Mann-Whitney's test.
508 Merge images show an overlay of GFP-Atg32$_{1-381}$ and liposomes fluorescence channels. OMM
509 GUVs were made with 69.9% DOPC, 10% DOPE, 10% DOPS, 5% cardiolipin, 5% DGS-
510 Ni^{+2}NTA, and 0.1% RhPE. Automix+PI3P were made of 43.2% PC, 19% PE, 32% PI, 5% PI3P
511 with 0.1% DiD. Liposomes were either sonicated to obtain 30-50nm curved liposomes or extruded
512 though a 1µm-filter.

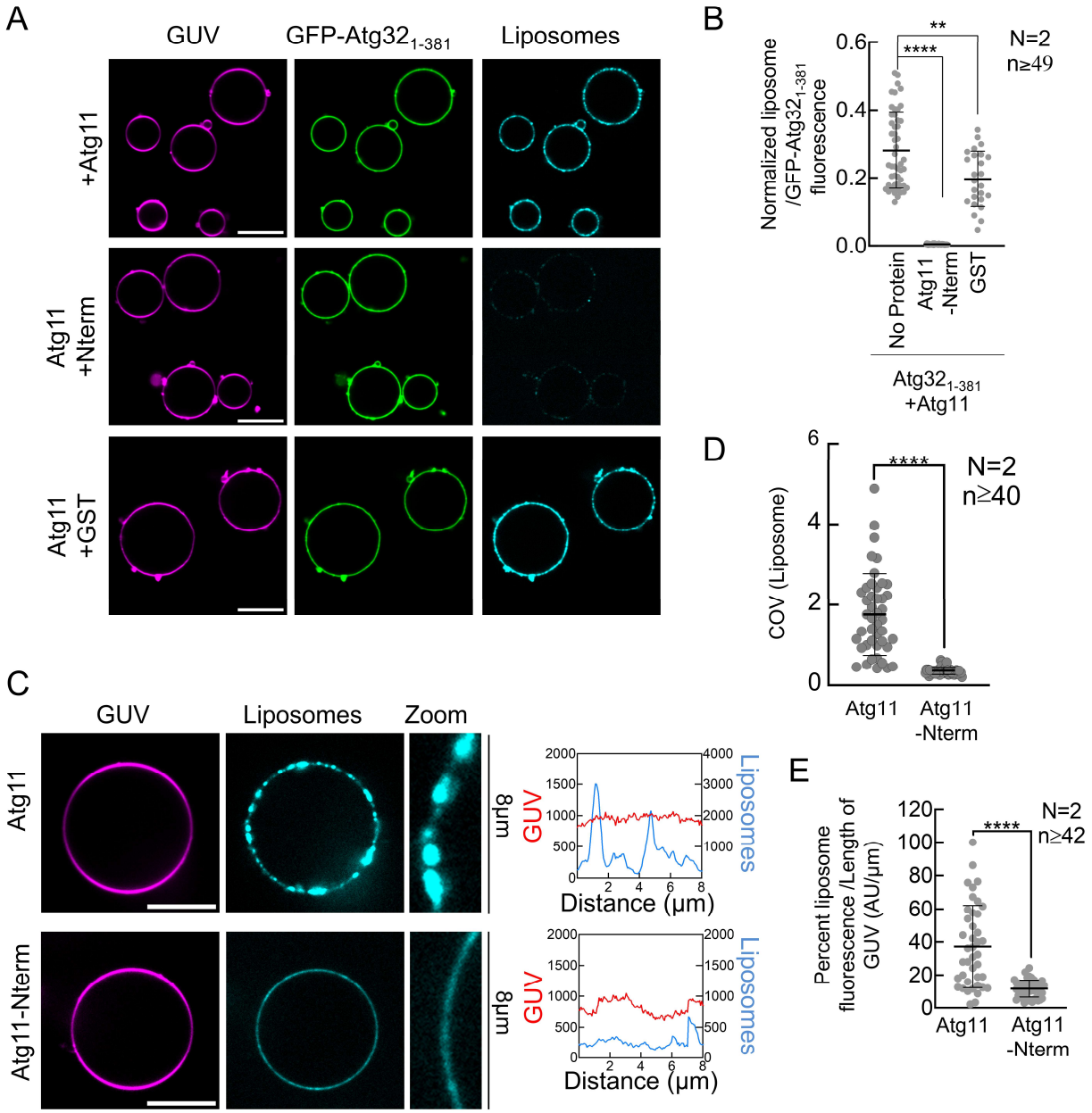

Figure 6. Membrane binding by Atg11-Nterm and self-association promotes autophagosomal vesicle tethering by Atg11. OMM GUVs containing mitochondrial lipids displaying GFP-Atg32$_{1-381}$ were incubated with Atg11 alone, Atg11 with 20-fold molar excess of Atg11-Nterm or GST and subsequently mixed with autophagosomal liposomes. (**A**) Representative images of autophagosomal liposome recruitment to mitochondrial GUVs with Atg11 alone, Atg11 with excess of Atg11-Nterm or Atg11 with excess of GST. Scale bar=10µm. (**B**) Quantification of the ratio of liposomes to GFP-Atg32$_{1-381}$ fluorescence from A. Data are presented as mean ± SD. **** indicates $p<0.0001$ and ** indicates $p<0.0026$ calculated using Mann-Whitney's test. N indicates number of independent repeats and n indicates the total number of GUVs analyzed per condition. (**C**) Representative images of autophagosomal liposome

524 recruitment to mitochondrial GUVs displaying GFP-Atg32$_{1-381}$ with Atg11 or GFP-Atg11-Nterm
525 alone (recruited via 6X-His tag). Scale bar=10µm. Fluorescence intensity profiles for the GUV
526 and liposome channels along the circumference of the GUV are shown to the right of each
527 representative image. (**D**) Quantification of the coefficient of variance (COV) for liposome
528 fluorescence along the circumference of the GUV from C. Data are presented as mean ± SD from
529 2 independent repeats (N=2). n indicates the total number of GUVs analyzed per condition. ****
530 indicates p<0.0001 analyzed using the non-parametric Mann-Whitney's test (**E**) Quantification of
531 the ratio of liposomes to GFP-Atg32$_{1-381}$ fluorescence from C. Data are presented as mean ± SD
532 from 2 independent repeats (N=2). n indicates the total number of GUVs analyzed per condition.
533 **** indicates p<0.0001 analyzed using non-parametric Mann-Whitney's test. OMM GUVs were
534 made with 69.9% DOPC, 10% DOPE, 10% DOPS, 5% cardiolipin, 5% DGS-Ni^{+2}NTA, and 0.1%
535 RhPE. Sonicated Automix+PI3P were made of 43.2% PC, 19% PE, 32% PI, 5% PI3P with 0.1%
536 DiD.

537

538

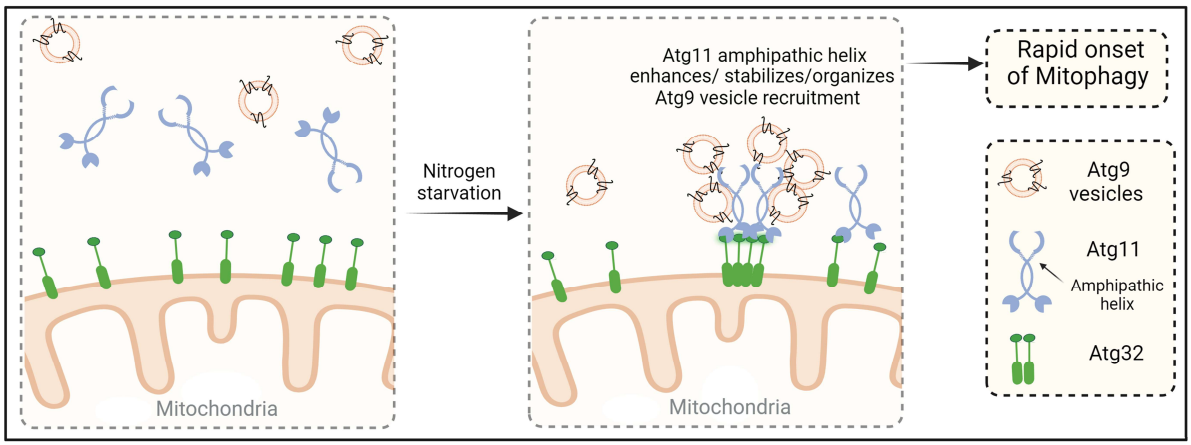

Figure 7. Proposed role of Atg11 membrane binding in mitophagy initiation. In response to nitrogen starvation, Atg32 recruits Atg11 to mitochondria leading to their clustering into mitophagy initiation sites. An amphipathic helix in Atg11 engages with negatively charged lipids in Atg9 vesicles. This membrane binding may serve to enhance, stabilize or organize the recruitment of Atg9 vesicles helping in rapid onset of mitophagy.

546 # MATERIALS AND METHODS

547 ## Recombinant protein expression and purification

548 All constructs used for protein purification in this paper are listed in **Table S1**. 6XHis-GST,
549 12XHis-GST-EEA1 FYVE, 12XHis-GST-GFP-EEA1 FYVE, and StrepII-GFP-Atg32(1-381)-
550 10XHis were recombinantly expressed in *E. coli* Star cells (Invitrogen C601003). Cultures were
551 grown in LB broth (Fisher Scientific, BP1426) to an OD600 of 0.6 to 0.8 at 37°C while shaking at
552 210 rpm. Cultures were cooled at 4°C for 20 min. Protein expression was induced by adding 1 mM
553 isopropylthio-β-D-galactopyranoside (IBI Scientific, IB02125) and the cultures were grown for an
554 additional 18 h at 18°C. Cells were harvested and cell pellets were stored at −80°C.

555

556 For purification of 6XHis-GST, 12XHis-GST-EEA1 FYVE, 12XHis-GST-GFP-EEA1 FYVE
557 and StrepII-GFP-Atg32(1-381)-10XHis, cell pellets were thawed and resuspended in 50 mM Tris
558 pH 8.0, 500 mM NaCl, 2.5mM imidazole, 5 mM $MgCl_2$, 1 mM phenylmethanesulfonyl fluoride
559 (PMSF; VWR, 0754) and cOmplete Mini EDTA-free protease inhibitor tablets (Roche,
560 11836170001). Cells were lysed using 3 strokes of a microfluidizer at 18, 000 psi. Triton X- 100
561 (VWR, AAA16046-AE), was subsequently added to lysates at 1% vol/vol. Lysates were spun at
562 25,000 g for 30 minutes. The supernatant was then applied to pre-equilibrated Talon resin
563 (Clontech, 635504). The resin was washed with 50 mM Tris pH 8.0, 500 mM NaCl, 10 mM
564 imidazole. Bound proteins were eluted with 50 mM Tris pH8.0, 500 mM NaCl, 250 mM imidazole.
565 For purification of 6XHis-GST, 12XHis-GST-EEA1 FYVE, 12XHis-GST-GFP-EEA1 FYVE,
566 peak fractions containing protein were pooled and dialyzed against 20 mM Tris pH 8.0, 300 mM
567 NaCl and 0.2 mM TCEP. Proteins were aliquoted, flash-frozen in liquid nitrogen and stored at
568 −80°C. For purification of StrepII-GFP-Atg32(1-381)- 10XHis, elutions from Talon resin were

569 pooled and incubated with pre- equilibrated Strep resin (IBA, 2-5030-025). The resin was washed
570 with 20 mM Tris pH 8.0 and 300 mM NaCl. Protein was eluted with 20 mM Tris pH 8.0, 300 mM
571 NaCl and 50 mM biotin. Peak fractions containing protein were dialyzed against 20 mM Tris pH
572 8.0, 300 mM NaCl and 0.2 mM TCEP. Dialyzed protein was aliquoted, flash-frozen in liquid
573 nitrogen and stored at −80°C until use.

574

575 Atg11 and GFP-Atg11, both with an N-terminal 2XStrep II tag, were recombinantly expressed in
576 Freestyle cells for 3 days post transfection. Cells were harvested by spinning by 1000 g for 15 min.
577 Cell pellets were flash frozen in liquid nitrogen and stored at −80°C.

578

579 Cell pellets were resuspended and thawed in 50 mM Tris pH 8.0, 500 mM NaCl, 1 mM DTT, 1
580 mM PMSF and a cOmplete Mini protease inhibitor tablet (Roche, 11836170001). Cells were lysed
581 using 3 strokes of a microfluidizer at 18, 000 psi. Triton X-100 (VWR, AAA16046-AE), was
582 subsequently added to lysates at 1% vol/vol. Lysates were spun at 25,000 g for 30 min. Supernatant
583 was applied to Strep resin (IBA, 2- 5030-025) at 1 mL/min using a peristaltic pump. Resin was
584 washed with 20 mM Tris pH 8.0, 300 mM NaCl and 1 mM DTT. Bound protein was eluted with
585 20 mM Tris pH 8.0, 300 mM NaCl, 50 mM biotin and 1 mM DTT. Fractions containing protein
586 were pooled and concentrated to 2 μM and flash-frozen in liquid nitrogen. For GFP-Atg32 binding
587 experiments, Atg11 was fluorescently labeled with a three-fold molar excess of Alexa Fluor™ 594
588 C5 Maleimide (Invitrogen, A10256) for 1 h at room temperature. Labelling was quenched using 1
589 mM DTT. Unreacted dye was removed by dialyzing the labelled protein against 20 mM Tris pH

590 8.0, 300 mM NaCl, 0.2 mM TCEP and 1 mM DTT for 48 h. Fresh buffer was added after 24 h of
591 dialysis.

592

593 The sequences encoding for Atg11 amino acids 1-646 (Nterm) and 700-1178 (Cterm) were
594 subcloned into pET His6 GFP TEV LIC cloning vector (1GFP) which was a gift from Scott Gradia
595 (Addgene plasmid # 29663) to generate GFP-Atg11-Nterm and GFP-Atg11-Cterm, respectively.
596 The sequence encoding for Atg11 amino acids 1-646 was also subcloned into pET His6 MBP TEV
597 LIC cloning vector (1M) which was a gift from Scott Gradia (Addgene plasmid # 29656). Q5
598 mutagenesis (NEB, E0554) was used to remove amino acids 612-646 from the Atg11-Nterm
599 constructs to generate Atg11-Nterm$^{\Delta 612\text{-}646}$ in the 1GFP and 1M vectors.

600

601 His6-GFP-Atg11-Nterm, His6-GFP-Atg11-Nterm$^{\Delta 612\text{-}646}$, His6-GFP-Atg11-Cterm, His6-MBP-
602 Atg11-Nterm and His6-MBP-Atg11- Nterm$^{\Delta 612\text{-}646}$ were all expressed in Rosetta2 *E. coli* cells.
603 Cells were grown to and OD_{600} of 0.5-0.6 and induced with 0.1mM IPTG (His6-GFP-Atg11-
604 Nterm, His6-GFP-Atg11-Nterm$^{\Delta 612\text{-}646}$, His6-GFP-Atg11-Cterm) or 1mM IPTG (His6-MBP-
605 Atg11-Nterm and His6-MBP-Atg11- Nterm$^{\Delta 612\text{-}646}$) and allowed to grow for 16 hours at 18°C.
606 Cells were then harvested by spinning at 4000 g for 25 minutes. Cell pellets were then flash frozen
607 in liquid nitrogen and stored at −80°C.

608

609 Cell pellets were resuspended in resuspended and thawed in 50 mM Tris pH 8.0, 500 mM NaCl,
610 5 mM $MgCl_2$, 1 mM PMSF and a cOmplete EDTA free Mini protease inhibitor tablet (Roche,
611 11836170001). Cells were lysed using 3 strokes of a microfluidizer at 18, 000 psi. Triton X-100

612 (VWR, AAA16046-AE), was subsequently added to lysates at 1% vol/vol. Lysates were spun at
613 40,000 g for 45 minutes. Supernatant was applied to TALON resin (Takara, 35653) and allowed
614 to incubate with gentle rocking for 1 hour. Supernatant was then allowed to slowly flow via gravity
615 and the resin was washed with 50 mM Tris pH 8.0, 300 mM NaCl three times followed by one
616 wash of 50 mM Tris pH 8.0, 300 mM NaCl, 2.5mM imidazole. Bound protein was eluted with 50
617 mM Tris pH 8.0, 300 mM NaCl, 200 mM imidazole. For, His6-MBP-Atg11-Nterm and His6-
618 MBP-Atg11- Nterm$^{\Delta 612\text{-}646}$ fractions containing protein were pooled and desalted into 50 mM Tris
619 pH 8.0, 300 mM NaCl and incubated with TEV protease at a 1:25 molar ratio at 4°C for 16 hours
620 to cleave off the His6-MBP tag. The cleaved protein was then subjected to size exclusion
621 chromatography using a HiLoad 16/60 Superdex 200 equilibrated with 20 mM Tris pH 7.4, 150
622 mM NaCl, 0.2 mM TCEP. Fractions containing Atg11-Nterm or Atg11- Nterm$^{\Delta 612\text{-}646}$ were then
623 concentrated and flash frozen until further use. For His6-GFP-Atg11-Nterm, His6-GFP-Atg11-
624 Nterm$^{\Delta 612\text{-}646}$ and His6-GFP-Atg11-Cterm fractions containing protein eluted from TALON resin
625 were pooled, concentrated and subjected to size exclusion chromatography using a HiLoad 16/60
626 Superdex 200 column equilibrated with 20 mM Tris pH 7.4, 150 mM NaCl, 0.2 mM TCEP.

627

628 Yeast strains, plasmids and culture conditions

629 *Atg11Δ* cell line was obtained from the *S. cerevisiae* knockout collection (Invitrogen). TKYM22
630 (SEY6210 OM45-GFP::TRP1) was a gift from Daniel Klionsky[44]. TKYM22 atg11Δ::NAT
631 (XXY003) was generated by replacing atg11 with the NAT cassette from pAG25 in TKYM22[27].

632 GFP-Atg32 and RFP-Atg32 (pRS415-MET25) plasmids were kind gifts from Dr. Benedikt
633 Westermann[45]. Plasmid expressing 2XGFP-Atg11 (yCPLAC33) and Atg11 (yCPLAC33) were

634 reported earlier[27]. Atg11$^{\Delta 612\text{-}646}$ was generated from Atg11 (yCPLAC33) by site directed
635 mutagenesis. Cells were grown in SMD (0.67% yeast nitrogen base, 2% glucose and supplemented
636 with the appropriate amino acid and vitamin mixture). CuGFP-ATG8(416) was a gift from Daniel
637 Klionsky (Addgene plasmid # 49423)[46].

638

639 Live imaging of GFP-Atg32 puncta formation

640 For GFP-Atg32 puncta formation experiments, cells expressing GFP-Atg32 under the MET25
641 promoter were grown to mid-log phase in SMD supplemented with 10 mg/mL methionine. GFP-
642 Atg32 expression was then induced by shifting cells to SMD without methionine for 1hr.
643 Subsequently, cells were transferred onto a concavalinA-coated glass coverslip assembled in a
644 temperature- and flow-controlled FCS2 chamber (Bioptechs). Chamber temperature was
645 maintained at 30 °C. To induce mitophagy, SD-N (0.17% yeast nitrogen base without amino acids
646 and ammonium sulfate; 2% glucose) prewarmed to 30 °C was flowed into the chamber at a
647 constant flowrate. Chamber was equilibrated with SD-N for 3 mins. Subsequently, timelapse
648 images were acquired at every 4 mins interval for a total of 30-40 mins.

649

650 OM45-GFP processing assay

651 The OM45-GFP processing assay was performed as described previously[31]. XXY003 cells were
652 transformed with Atg11 and Atg11$^{\Delta 612\text{-}646}$. Cells were grown at 30 °C in SMD to an OD600 of 0.8–
653 1.0. Cells were pelleted at 1000*g* for 10 min, washed and resuspended in SML (0.67% yeast
654 nitrogen base, 2% lactic acid and supplemented with the appropriate amino acid and vitamin

655 mixture) and grown for 16 hrs. Subsequently, cells were pelleted and resuspended in SD-N for 6
656 h. Finally, cells were harvested, lysed by bead beating and GFP was detected by western blot.

657

658 **Liposome preparation**

659 All lipids were purchased from Avanti Polar lipids. Chloroform stocks of lipid mixtures at a desired
660 ratio containing 0.1 mol% of the fluorescent lipophilic dye DiD were aliquoted in a clean glass
661 tube and dried under a gentle nitrogen stream until all the chloroform had evaporated. Residual
662 chloroform was removed under vacuum for 18 h. Dried lipids were resuspended in 20 mM Tris
663 pH 8.0, 150 mM NaCl to a final concentration of 1 mM. For experiments with Atg11,
664 automix+PI3P liposomes were resuspended in 20 mM Tris pH 8.0, 100 mM NaCl to a final
665 concentration on 1 mM. Liposomes were extruded using an Avanti Mini Extruder using 0.4 μm
666 Nuclepore Track-Etched membrane (Sigma Aldrich, WHA10417104). Automix+PI3P liposomes
667 were sonicated using a probe sonicator at 10% amplitude for 5 mins with 1 sec on and 1 sec off.
668 Sonication was carried out in an ice-water bath to prevent heating.

669

670 **Giant unilamellar vesicle preparation**

671 GUVs were made using the gel-assisted formation method[51]. Briefly, chloroform stocks containing
672 lipids mixed at desired ratios containing the fluorescent lipid RhPE were aliquoted in a glass tube.
673 Chloroform was dried under a stream of nitrogen followed by drying under vacuum (1 h). The
674 dried lipids were resuspended in fresh chloroform to make a 1 mM lipid mixture. Polyvinyl alcohol
675 (PVA, Mw = 14500; Sigma, 814894) was dissolved in boiling water to make a 5% stock and

676 degassed in a vacuum chamber. PVA solution (10 μL) was spread into a thin film on a glass
677 coverslip kept on a heating block set to 55°C. Chloroform-dissolved lipid mix (10 μL) was then
678 spread on the dried PVA film. The dried PVA-lipid films were peeled from the glass coverslips
679 and transferred to a 1.5-mL microcentrifuge tube. Films were hydrated in 300 μL assay buffer (20
680 mM Tris, pH 7.4, 150 mM NaCl) for 20 min, and GUVs were released by gentle tapping. The
681 PVA films were removed using a pipette.

682

683 **GUV liposome tethering (GLT)**

684 For GLT experiments, GUVs were first mixed with tethering protein or control protein in a 1.5
685 mL microcentrifuge tube for 10 minutes at room temperature. GUV mixtures were tapped to
686 resuspend settled GUVs and subsequently incubated with 10 μL of 400 nm extruded liposomes for
687 5mins at room temperature. Liposomes were used within 3 days of extrusion. The GLT mixtures
688 (300 μL total volume) were transferred to a BSA-passivated LabTek chamber (Nunc, Z734853)
689 for imaging. GUVs were allowed to settle for 5 minutes prior to imaging. LabTek chambers were
690 treated with 3 M NaOH for 10 minutes followed by extensive washes with milliQ water. NaOH-
691 treated chambers were then passivated by incubation with BSA (3 mg/mL). BSA was removed by
692 three washes with the assay buffer. All GLT experiments were performed in 20 mM Tris pH 7.4,
693 150 mM NaCl, except for GLT experiments with Atg11 which were performed in 20 mM Tris pH
694 7.4, 100 mM NaCl. All proteins were spun at 100,000 g prior to use to remove any aggregates.

695

696 **Atg11 binding on SMrTs**

697 SMrTs were prepared as described earlier[22,23]. Briefly, 3 μL of chloroform-dissolved automix and
698 automix+PI3P stocks (1mM) were spread on a PEGylated coverslip. Chloroform was dried using
699 a gentle stream of nitrogen. A ~35 μL flow cell (Bioptechs) was assembled by placing a 0.1 mm
700 silicone spacer between the PEGylated coverslip and an ITO-coated slide. Rehydration of the dried
701 lipid film with 20mM Tris pH 8 and 150mM NaCl yielded supported lipid bilayers and vesicles.
702 Lipid nanotubes were extruded from the vesicles using buffer flow. Subsequently, 300 μL of GFP-
703 Atg11 (0.5 μM), GFP-Atg11-Nterm (2 μM) or GFP-Atg11-Cterm (2 μM) were incubated with
704 SMrTs for 10 mins. Excess protein was washed with 3x300 μL of buffer and SMrTs were imaged.
705 All proteins were spun at 100,000 g prior to use to remove any aggregates.

706

707 Fluorescence microscopy of membrane binding and GLT

708 All images were acquired using a Nikon TiE microscope fitted with a Yokogawa CSU-W1
709 spinning disk system using a 100 X, 1.45 NA oil immersion objective. Images were acquired with
710 a Photometrics Prime BSI sCMOS camera using the NIS elements software.

711

712 Atg11 Clustering Assay

713 All buffers used for these assays contained 20 mM Tris pH 8.0 at 4ºC and the indicated NaCl
714 concentrations. Purified GFP-Atg11 was thawed on ice and centrifuged at 20,000 x g for 15
715 minutes at 4ºC. GFP-Atg11 was diluted to a concentration of 1 μM in buffer containing 50, 100,
716 150, 300 or 450 mM NaCl, or to a concentration of 0.05, 0.1, 0.5, 1 or 5 μM in buffer containing
717 150 mM NaCl. After dilution 40 μl of sample was spotted onto a glass coverslip, mounted on a 63

718 X oil immersion objective on a Zeiss LSM 880 microscope. Samples were left on the microscope
719 for 5 minutes before imaging. All images were acquired within 10 minutes after the sample was
720 applied to the coverslip to prevent evaporation and thus concentration of the sample. For
721 reversibility assays, GFP-Atg11 was diluted to 1μM in buffer containing 150 mM NaCl or 450
722 mM NaCl and imaged as described above. The remaining samples of 1μM GFP-Atg11 in 150 mM
723 NaCl and 450 mM NaCl were mixed in a 1:1 ratio to generate 1μM GFP-Atg11 in 300 mM NaCl.
724 For the comparison of GFP-Atg11, GFP-Atg11-Nterm and GFP-Atg11-Cterm protein was diluted
725 to 1 μM in buffer containing 150 mM NaCl and imaged as described above.

726

727 Atg11 clustering was imaged on a Zeiss Airyscan LSM 880 microscope using an alpha Plan-
728 Apochromatic 100 × oil lens with NA = 1.46 using Zeiss Immersol 518 F immersion oil at room
729 temperature. GFP was excited using a 488 argon laser. Emission was detected using a Zeiss
730 GaAsP-PMT detector.

731

732 Image analysis

733 Fluorescence microscopy images were analyzed using Fiji[52].

734 To analyze tethering in GLT, images were first background corrected by subtracting the mode
735 intensity value. Percent liposome fluorescence per length of GUV was calculated by normalizing
736 the liposome fluorescence, collected from a two-pixel wide segmented line drawn along a GUV,
737 to the length of the GUV. For calculating the liposome/protein fluorescence ratio, fluorescence
738 intensities in liposome and protein channels from a two-pixel wide segmented line drawn along a

739 GUV were collected. Mean liposome fluorescence was divided by mean protein fluorescence to
740 yield liposome/protein fluorescence ratios.

741

742 For analysis of protein bound on SMrTs, images were background corrected by subtracting the
743 mode value. Integrated density of protein and membrane fluorescence was measured from a 20x10
744 pixel rectangle placed centrally on the tubes or from a 2 to 4 μm^2 square box placed on SLBs.

745 GFP-Atg32 puncta were analyzed by placing a segmented line centered on the puncta. Only those
746 GFP-Atg32 puncta that were over 2.5-fold intensity of the background mitochondrial fluorescence
747 intensity were counted.

748

749 For Atg11 clustering analysis images were analyzed in Fiji. A threshold was set for each image
750 based on the average background intensity of the image. The analyze particle command was used
751 with parameters of 0.2 µm to infinity for the particle size and 0.8-1.0 for the circularity.

752

753 **Statistical analysis**

754 Statistical analysis was performed using GraphPad Prism (version 5.0a).

755 All experiments were performed in independent triplicates or duplicates. Liposomes and GUVs
756 were prepared independently for each GLT experiment using freshly aliquoted lipids. Data from
757 all repeats were pooled and plotted as scatterplots. Error bars represent standard deviation.
758 Significance was calculated using the non-parametric Mann-Whitney's test or one-way ANOVA
759 with Tukey's correction for multiple comparisons as appropriate.

760

761 ## AUTHOR CONTRIBUTIONS

762 D.A., S.K., K.M.B., and M.J.R. conceived and planned the experiments. D.A., S.K., S.I.N. and
763 K.M.B. carried out the experiments. D.A. and M.J.R. drafted the manuscript. All authors edited
764 the manuscript.

765

766 ## ACKNOWLEDGMENTS

767 This work was supported by the National Institute of General Medical Sciences (NIGMS) grant
768 R35GM128663 to M.J.R. Expression of Atg11 was performed in the BioMT service center and
769 protein purification was performed in part performed at the BioMT Molecular Tools Core which
770 are both supported by NIGMS grant P20GM113132. Sequencing of plasmids was performed by
771 the Molecular Biology Shared Resource Center which is supported by NCI Cancer Center Support
772 Grant P30CA023108. We would also like to thank Ann Lavanway for her work and support at the
773 Dartmouth Imaging Facility. We thank Dr. Benedikt Westermann for the kind gift of GFP-Atg32
774 and RFP-Atg32 pRS415-MET25 plasmids.

775

REFERENCES

1. Wen X, Klionsky DJ. An overview of macroautophagy in yeast. J Mol Biol 2016; 428:1681-99. doi:10.1016/j.jmb.2016.02.021.
2. Germic N, Frangez Z, Yousefi S, Simon HU. Regulation of the innate immune system by autophagy: monocytes, macrophages, dendritic cells and antigen presentation. Cell Death Differ 2019; 26:715-27. doi:10.1038/s41418-019-0297-6.
3. Dikic I, Elazar Z. Mechanism and medical implications of mammalian autophagy. Nat Rev Mol Cell Biol 2018; 19:349-64. doi:10.1038/s41580-018-0003-4.
4. Lamark T, Johansen T. Mechanisms of Selective Autophagy. Annu Rev Cell Dev Biol 2021; 37:143-69. doi:10.1146/annurev-cellbio-120219-035530.
5. Adriaenssens E, Ferrari L, Martens S. Orchestration of selective autophagy by cargo receptors. Current Biology 2022; 32:R1357-R71. doi:10.1016/j.cub.2022.11.002.
6. Yorimitsu T, Klionsky DJ. Atg11 links cargo to the vesicle-forming machinery in the cytoplasm to vacuole targeting pathway. Mol Biol Cell 2005; 16:1593-605. doi:10.1091/mbc.e04-11-1035.
7. Matscheko N, Mayrhofer P, Rao Y, Beier V, Wollert T. Atg11 tethers Atg9 vesicles to initiate selective autophagy. PLoS Biol 2019; 17:e3000377. doi:10.1371/journal.pbio.3000377.
8. Coudevylle N, Banas B, Baumann V, Schuschnig M, Zawadzka-Kazimierczuk A, Kozminski W, et al. Mechanism of Atg9 recruitment by Atg11 in the cytoplasm-to-vacuole targeting pathway. J Biol Chem 2022; 298:101573. doi:10.1016/j.jbc.2022.101573.
9. Sawa-Makarska J, Baumann V, Coudevylle N, von Bülow S, Nogellova V, Abert C, et al. Reconstitution of autophagosome nucleation defines Atg9 vesicles as seeds for membrane formation. Science 2020; 369:1206-+. doi:ARTN eaaz771410.1126/science.aaz7714.
10. Mari M, Griffith J, Rieter E, Krishnappa L, Klionsky DJ, Reggiori F. An Atg9-containing compartment that functions in the early steps of autophagosome biogenesis. J Cell Biol 2010; 190:1005-22. doi:10.1083/jcb.200912089.
11. Melia TJ, Lystad AH, Simonsen A. Autophagosome biogenesis: From membrane growth to closure. J Cell Biol 2020; 219. doi:10.1083/jcb.202002085.
12. Maeda S, Otomo C, Otomo T. The autophagic membrane tether ATG2A transfers lipids between membranes. Elife 2019; 8. doi:ARTN e4577710.7554/eLife.45777.
13. Valverde DP, Yu S, Boggavarapu V, Kumar N, Lees JA, Walz T, et al. ATG2 transports lipids to promote autophagosome biogenesis. J Cell Biol 2019; 218:1787-98. doi:10.1083/jcb.201811139.
14. Jiang W, Chen X, Ji C, Zhang W, Song J, Li J, et al. Key Regulators of Autophagosome Closure. Cells 2021; 10. doi:10.3390/cells10112814.
15. He C, Song H, Yorimitsu T, Monastyrska I, Yen WL, Legakis JE, et al. Recruitment of Atg9 to the preautophagosomal structure by Atg11 is essential for selective autophagy in budding yeast. J Cell Biol 2006; 175:925-35. doi:10.1083/jcb.200606084.
16. Meyer MD, Winzeler J, Taylor SM, Kilgore A, Edicha K, Chitwood C, et al. Mapping Critical Residues in ATG11's Coiled-Coil 2 Domain that Block Multiple Interactions and Disrupt Selective Autophagy. Front Cell Dev Biol 2021; 9:775364. doi:10.3389/fcell.2021.775364.

820 17. Shi X, Chang C, Yokom AL, Jensen LE, Hurley JH. The autophagy adaptor NDP52 and
821 the FIP200 coiled-coil allosterically activate ULK1 complex membrane recruitment. Elife
822 2020; 9. doi:10.7554/eLife.59099.
823 18. Suzuki H, Noda NN. Biophysical characterization of Atg11, a scaffold protein essential for
824 selective autophagy in yeast. FEBS Open Bio 2018; 8:110-6. doi:10.1002/2211-
825 5463.12355.
826 19. Schutter M, Giavalisco P, Brodesser S, Graef M. Local Fatty Acid Channeling into
827 Phospholipid Synthesis Drives Phagophore Expansion during Autophagy. Cell 2020;
828 180:135-49 e14. doi:10.1016/j.cell.2019.12.005.
829 20. Hawkins WD, Leary KA, Andhare D, Popelka H, Klionsky DJ, Ragusa MJ. Dimerization-
830 dependent membrane tethering by Atg23 is essential for yeast autophagy. Cell Rep 2022;
831 39:110702. doi:10.1016/j.celrep.2022.110702.
832 21. Popelka H, Reinhart EF, Metur SP, Leary KA, Ragusa MJ, Klionsky DJ. Membrane
833 Binding and Homodimerization of Atg16 Via Two Distinct Protein Regions is Essential
834 for Autophagy in Yeast. J Mol Biol 2021; 433:166809. doi:10.1016/j.jmb.2021.166809.
835 22. Dar S, Kamerkar SC, Pucadyil TJ. A high-throughput platform for real-time analysis of
836 membrane fission reactions reveals dynamin function. Nat Cell Biol 2015; 17:1588-96.
837 doi:10.1038/ncb3254.
838 23. Dar S, Kamerkar SC, Pucadyil TJ. Use of the supported membrane tube assay system for
839 real-time analysis of membrane fission reactions. Nat Protoc 2017; 12:390-400.
840 doi:10.1038/nprot.2016.173.
841 24. Yamamoto H, Kakuta S, Watanabe TM, Kitamura A, Sekito T, Kondo-Kakuta C, et al.
842 Atg9 vesicles are an important membrane source during early steps of autophagosome
843 formation. J Cell Biol 2012; 198:219-33. doi:10.1083/jcb.201202061.
844 25. Shi X, Yokom AL, Wang C, Young LN, Youle RJ, Hurley JH. ULK complex organization
845 in autophagy by a C-shaped FIP200 N-terminal domain dimer. J Cell Biol 2020; 219.
846 doi:10.1083/jcb.201911047.
847 26. Jumper J, Evans R, Pritzel A, Green T, Figurnov M, Ronneberger O, et al. Highly accurate
848 protein structure prediction with AlphaFold. Nature 2021; 596:583-9. doi:10.1038/s41586-
849 021-03819-2.
850 27. Margolis HK, Katzenell S, Leary KA, Ragusa MJ. The Third Coiled Coil Domain of Atg11
851 Is Required for Shaping Mitophagy Initiation Sites. J Mol Biol 2020; 432:5752-64.
852 doi:10.1016/j.jmb.2020.08.025.
853 28. Turco E, Witt M, Abert C, Bock-Bierbaum T, Su MY, Trapannone R, et al. FIP200 Claw
854 Domain Binding to p62 Promotes Autophagosome Formation at Ubiquitin Condensates.
855 Mol Cell 2019; 74:330-46 e11. doi:10.1016/j.molcel.2019.01.035.
856 29. Gallop JL, Jao CC, Kent HM, Butler PJ, Evans PR, Langen R, et al. Mechanism of
857 endophilin N-BAR domain-mediated membrane curvature. EMBO J 2006; 25:2898-910.
858 doi:10.1038/sj.emboj.7601174.
859 30. Nishimura T, Lazzeri G, Mizushima N, Covino R, Tooze SA. Unique amphipathic helix
860 drives membrane insertion and enzymatic activity of ATG3. Sci Adv 2023; 9. doi:ARTN
861 eadh128110.1126/sciadv.adh1281.
862 31. Kanki T, Kang D, Klionsky DJ. Monitoring mitophagy in yeast: the Om45-GFP processing
863 assay. Autophagy 2009; 5:1186-9. doi:10.4161/auto.5.8.9854.

32. Kanki T, Wang K, Cao Y, Baba M, Klionsky DJ. Atg32 is a mitochondrial protein that confers selectivity during mitophagy. Dev Cell 2009; 17:98-109. doi:10.1016/j.devcel.2009.06.014.
33. Okamoto K, Kondo-Okamoto N, Ohsumi Y. Mitochondria-anchored receptor Atg32 mediates degradation of mitochondria via selective autophagy. Dev Cell 2009; 17:87-97. doi:10.1016/j.devcel.2009.06.013.
34. Aoki Y, Kanki T, Hirota Y, Kurihara Y, Saigusa T, Uchiumi T, et al. Phosphorylation of Serine 114 on Atg32 mediates mitophagy. Mol Biol Cell 2011; 22:3206-17. doi:10.1091/mbc.E11-02-0145.
35. Hollenstein DM, Licheva M, Konradi N, Schweida D, Mancilla H, Mari M, et al. Spatial control of avidity regulates initiation and progression of selective autophagy. Nat Commun 2021; 12:7194. doi:10.1038/s41467-021-27420-3.
36. Fujioka Y, Alam JM, Noshiro D, Mouri K, Ando T, Okada Y, et al. Phase separation organizes the site of autophagosome formation. Nature 2020; 578:301-5. doi:10.1038/s41586-020-1977-6.
37. Chang C, Shi X, Jensen LE, Yokom AL, Fracchiolla D, Martens S, et al. Reconstitution of cargo-induced LC3 lipidation in mammalian selective autophagy. Sci Adv 2021; 7. doi:10.1126/sciadv.abg4922.
38. Turco E, Savova A, Gere F, Ferrari L, Romanov J, Schuschnig M, et al. Reconstitution defines the roles of p62, NBR1 and TAX1BP1 in ubiquitin condensate formation and autophagy initiation. Nat Commun 2021; 12:5212. doi:10.1038/s41467-021-25572-w.
39. Alam JM, Noda NN. In vitro reconstitution of autophagic processes. Biochem Soc Trans 2020; 48:2003-14. doi:10.1042/BST20200130.
40. Dumas JJ, Merithew E, Sudharshan E, Rajamani D, Hayes S, Lawe D, et al. Multivalent endosome targeting by homodimeric EEA1. Mol Cell 2001; 8:947-58. doi:10.1016/s1097-2765(01)00385-9.
41. Song H, Wickner W. Tethering guides fusion-competent trans-SNARE assembly. Proc Natl Acad Sci U S A 2019; 116:13952-7. doi:10.1073/pnas.1907640116.
42. Sperka-Gottlieb CD, Hermetter A, Paltauf F, Daum G. Lipid topology and physical properties of the outer mitochondrial membrane of the yeast, Saccharomyces cerevisiae. Biochim Biophys Acta 1988; 946:227-34. doi:10.1016/0005-2736(88)90397-5.
43. Gatica D, Damasio A, Pascual C, Klionsky DJ, Ragusa MJ, Popelka H. The carboxy terminus of yeast Atg13 binds phospholipid membrane via motifs that overlap with the Vac8-interacting domain. Autophagy 2020; 16:1007-20. doi:10.1080/15548627.2019.1648117.
44. Kanki T, Klionsky DJ. Mitophagy in Yeast Occurs through a Selective Mechanism. Journal of Biological Chemistry 2008; 283:32386-93. doi:10.1074/jbc.M802403200.
45. Bockler S, Westermann B. Mitochondrial ER contacts are crucial for mitophagy in yeast. Dev Cell 2014; 28:450-8. doi:10.1016/j.devcel.2014.01.012.
46. Wang K, Yang Z, Liu X, Mao K, Nair U, Klionsky DJ. Phosphatidylinositol 4-kinases are required for autophagic membrane trafficking. J Biol Chem 2012; 287:37964-72. doi:10.1074/jbc.M112.371591.